

TEMPERATURE DEPENDENCE OF THE COHERENCE IN POLARITON CONDENSATES

E. Rozas^{1,2}, M.D. Martín^{1,2}, C. Tejedor^{2,3,4}, L. Viña^{1,2,4}, and G. Deligeorgis⁵,
Z. Hatzopoulos⁵ and P.G. Savvidis^{5,6,7}

¹*Dept. Física de Materiales & Inst. N. Cabrera, Univ. Autónoma, Madrid 28049, Spain*

²*Instituto Nicolás. Cabrera, Univ. Autónoma, Madrid 28049, Spain*

³*Dept. Física Teórica de la Materia Condensada. Univ. Autónoma, Madrid 28049. Spain*

⁴*Inst. de Física de la Materia Condensada, Universidad Autónoma, Madrid 28049, Spain*

⁵*FORTH-IESL, P.O. Box 1385, 71110 Heraklion, Crete, Greece*

⁶*Dept. of Materials Science & Technology, University of Crete, 71003 Heraklion, Greece*

⁷*ITMO University, St. Petersburg 197101, Russia*

We present a time-resolved experimental study of the temperature effect on the coherence of travelling polariton condensates. The simultaneous detection of their emission both in real- and reciprocal-space allows us to fully monitor the condensates' dynamics. We obtain fringes in reciprocal-space as a result of the interference between polariton wavepackets (WPs) travelling with the swpsame speed. The periodicity of these fringes is inversely proportional to the spatial distance between the interfering WPs. In a similar fashion, we obtain interference fringes in real-space when WPs travelling in opposite directions meet. The visibility of both real- and reciprocal-space interference fringes rapidly decreases with increasing temperature and vanishes. A theoretical description of the phase transition, considering the coexistence of condensed and non-condensed particles, for an out of equilibrium condensate such as ours is still missing. Yet a comparison with theories developed for atomic condensates allows us to infer a critical temperature for the BEC-like transition when the visibility goes to zero.

I. INTRODUCTION

At low temperature, the optical properties of semiconductor crystals are dominated by exciton-polaritons, which are half-light, half-matter particles, resulting from the strong coupling between exciton and photon states [1]. Since their observation by Weisbuch *et al.* in semiconductor microcavities [2], polaritons in confined, low-dimensional structures have been profusely investigated. The strong light-matter coupling in the cavities gives rise to fascinating new effects that make polaritons appropriate candidates for nonlinear optical technologies [3]. Their excitonic part leads to strong polariton-polariton Coulomb interactions; furthermore, thanks to their photonic content, they can be easily created, by excitation with laser sources, and detected through the photon emission when polaritons annihilate. Their bosonic nature, together with their low effective mass and reduced density of states, facilitate their condensation in a macroscopic coherent phase that presents high similarities to

Bose-Einstein condensates (BECs) [4]. Coherence is a key ingredient of condensates, and has been intensely studied both in atomic BECs [5], and in polariton condensates [6-23]. The coherence has been mostly investigated in real-space, by studying interference effects, either for static condensates [11, 24, 25] or for moving ones when they meet in real-space [10, 26]. Notwithstanding, a recent experimental study has focused on the study of coherence when two condensates, that move with the same speed, interfere in momentum (k)-space [27], circumventing the need of an encounter in real-space. Antón *et al.* showed the presence of interference fringes produced by the correlation between two components of such condensates that were spatially separated by 70 μm , demonstrating the existence of remote coherence between these condensates. Generally, the study of coherence has been performed at temperatures well below the critical temperature for condensation (T_c), to optimize the creation and

stability of the condensates. To the best of our knowledge, only Bloch *et al.* [28] and Gati *et al.* [29, 30] have investigated the degree of spatial coherence as a function of T , in trapped atomic condensates. Analogous theoretical studies in the field of polariton condensates have been done [31]. Actually, the study of temperature dependence is arousing great interest in the field of polariton condensates. Lebedev *et al.* have analyzed the effect of finite temperature on the coupling of quasi-equilibrium exciton-polariton condensates in a Josephson junction: they describe a second order phase transition between classical (thermal) and quantum regimes characterized by a temperature parameter related to the polariton-polariton interaction length [32]. Moreover, another recent experiment by Ouellet-Plamondon *et al.* also gives the possibility to evaluate T_C [33]. They reported on the dependence of polariton bistability with temperature, proposing that an increase in T leads to a significant incoherent population growth in the reservoir, which interacts with the polariton population. The study showed a collapse of the polariton hysteresis loop as well as a decrease of the transmitted intensity above the upward threshold of the hysteresis loops for a temperature of ~ 22 K, revealing a strong loss of the coherent polariton population with increasing temperature. Here, we investigate the temperature dependence of the degree of coherence of polariton condensates in semiconductor microcavity ridges by a detailed analysis of interference patterns. Our measurements show a loss of coherence with increasing temperature both in real- and k -space.

II. EXPERIMENTAL RESULTS AND DISCUSSION

The sample used in this work is a high-quality, Q -factor ~ 16000 , GaAs-based 1D-microcavity, surrounded by two Bragg mirrors. On its surface, a pattern has been sculpted throughout the sample, consisting in ridge structures with dimensions $20\text{ }\mu\text{m} \times 300\text{ }\mu\text{m}$. Further details about the sample can be found in Ref. [34, 35]. It is kept in a variable-temperature cryostat under high vacuum conditions. The temperature dependence of the degree of coherence is studied from 10 K up to a temperature of 42.5 K.

To study the coherence of the condensates, we excite the sample with 2 ps-long light pulses from a Ti:Al₂O₃ laser source. The laser beam is divided into two, which are focused on the sample through a microscope objective. Both beams are precisely controlled to have the same power density; they arrive simultaneously, impinging at the same angle, and are separated by $d = 70(1)\text{ }\mu\text{m}$ on the sample surface. We adjust the optical excitation so that particles are initially created with $k_{\parallel} \sim 0$. The angle of detection (θ) is directly related to the parallel component of the polariton momentum, k_{\parallel} , by $k_{\parallel} = n \frac{2\pi}{\lambda} \sin \theta$.

Low temperature (10 K) continuous wave photoluminescence (PL) measurements (not shown) reveal that the emission spectrum of the sample is composed of a broad band between 1.5480 eV and 1.5420 eV, originating from the excitonic recombination [36] together with several narrow lower polariton branches (LPBs), between 1.5420 eV and 1.5398 eV, arising from the confinement along the narrow dimension of the ridge. Under resonant excitation conditions the phase of the polariton condensates would be inherited from that of the laser pulses, therefore to study the genuine condensates' coherence we excite quasi-resonantly, at 1.5459 eV. More details of the excitation conditions are reported in Ref [27]. The time-resolved PL is measured at the energy of traveling polaritons (1.5404 eV with a resolution of 0.45 meV), using a streak camera with an overall time-resolution of ~ 10 ps, averaging over millions of laser pulses. We obtain emission maps vs. position and time focusing the emission directly onto the entrance slit of a spectrometer connected to the streak camera. We are also able to record the PL vs. momentum and time, with the aid of an additional lens in our setup, collecting the light distribution in the Fourier plane of the microscope objective [27].

For excitation densities above threshold for polariton condensation, and after energy relaxation, polaritons with $k \sim 0$ evolve towards two states with momenta $\pm k$. As a result, the condensates propagate on both sides, away from the excitation spots [37,38]. This dynamics under the two-beam excitation conditions used in our

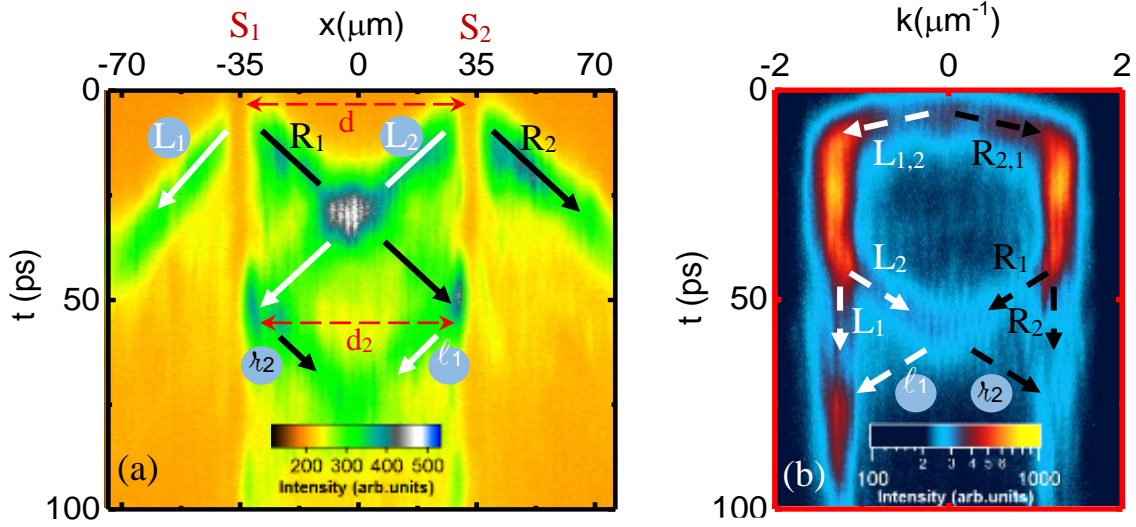


Figure 1. (a) PL emission along the ridge in real-space (x) as a function of time for $T = 14$ K. $S_{1,2}$ mark the positions where the two laser beams impinge on the sample. L_i (R_i) denote the WPs moving to the left (right), with the subscript, i , referring to the excitation beam. The red dashed arrow at the top of the image represents the spatial separation (d) between both beams at $t = 0$ while the arrow at ~ 55 ps marks the separation (d_2) between WPs R_1 and L_2 when they arrive at the excitonic reservoirs. The intensity is in a linear false-color scale. (b) The corresponding emission in momentum-space (k) as a function of time. The color of the arrows refers to the WPs described in (a). In this case, the intensity is in a logarithmic false-color scale. Both PL emissions have been measured with a power density of 6 kW/cm^2 .

experiments is compiled in Fig. 1, which depicts the emission maps both in real- and momentum-space. In real-space, [Fig. 1(a)], two polariton wave packets (WPs) arise from each excitation spot (S_1 @ $-35 \mu\text{m}$ and S_2 @ $+35 \mu\text{m}$), which move in opposite directions. We label these four WPs as L_i/R_i , as they move away from the excitation area S_i ($i=1, 2$) towards the left/right respectively. The WPs move with a constant speed of $\sim 1.5 \mu\text{m/ps}$ and their emission can be monitored up to ~ 130 ps. The outermost WPs, L_1 and R_2 , exit the detection window after 45 ps and therefore their PL cannot be measured from there on. The other two WPs, R_1 and L_2 , moving towards each other, meet in real-space ($x \sim 0$) at ~ 35 ps and interfere with each other, as evidenced by the interference fringes. At later times, R_1 and L_2 , continue travelling toward S_2 and S_1 , reaching the vicinity of these positions ($x \sim \pm 35 \mu\text{m}$) at ~ 55 ps. There, the potential walls created by the excitonic reservoirs [37,38] act as barriers that the WPs cannot overcome, decelerating and eventually stopping and reversing their trajectories, so that R_1 (L_2) becomes ℓ_1 (r_2). The separation between L_2 and

R_1 at this time, d_2 , is slightly smaller than d because the WPs are not able to reach the maxima of the barriers. Fig. 1(b) shows the corresponding time evolution of the WPs in momentum-space. Initially, the condensates accelerate from rest ($k = 0$) and they move left (right), reaching $k = -1.3 \mu\text{m}^{-1}$ ($k = +1.3 \mu\text{m}^{-1}$) in few picoseconds. The WPs travel with this wave vector up to ~ 40 ps. The left (right) trace reflects the movement of L_1 and L_2 (R_1 and R_2), respectively. From there on L_2 and R_1 start to decelerate, due to the presence of the excitonic reservoir potentials. Consequently, when the polaritons reach the vicinity of S_1 and S_2 ($t \sim 55$ ps) and stop, the traces merge at $k \sim 0$. Later on, the WPs reverse their movement direction [L_2 (R_1) becomes r_2 (ℓ_1)] and accelerate again until they attain the same momentum of the outermost WPs, $k = \pm 1.3 \mu\text{m}^{-1}$. We observe interference fringes during the first ~ 40 ps, both at negative and positive values of k , and later on, at ~ 55 ps and $k \sim 0$. The former ones arise from the fact that L_1 and L_2 (R_1 and R_2) increase their speed with the same acceleration, therefore traveling with the same momentum until they reach $-1.3 \mu\text{m}^{-1}$

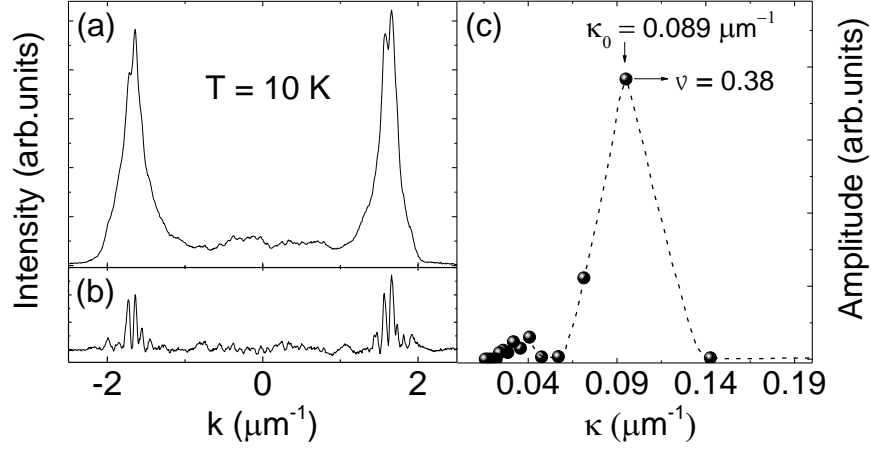


Figure 2. (a) PL emission in momentum-space time-integrated for t_1 at a temperature of 10 K. (b) Interferogram profile after a baseline subtraction of the trace shown in (a). (c) Amplitude of the different contributions to the interferogram obtained from a Fourier analysis of the trace depicted in (b): the value of the main period of the interference fringes is marked as κ_0 ; the corresponding visibility as v . The dashed line shows a Bézier interpolation of the points. A $10\text{kW}/\text{cm}^2$ excitation laser was used in the measurements.

($+1.3 \mu\text{m}^{-1}$), fulfilling the requirements for interference in k -space. To observe these fringes, it is crucial to assure the same conditions for each excitation spot, creating equal excitonic populations that lead to equal kinetics and consequently equal momenta (i.e. overlapping of the wave vectors in k -space) of the WPs traveling in the same direction. It also requires keeping a constant distance between the beams in real-space, since it determines the period of the interference patterns, as will be discussed below. The second set of fringes (at $t \sim 55$ ps) appear when R_1 and L_2 have both very low speed in the environs of the excitonic reservoirs ($S_{2,1}$). From then on, the polariton finite lifetime starts to hinder the detection of the condensates' emission. However, interferences are still observable for those polaritons moving to the left when the outermost WP L_1 merges with ℓ_1 .

Now, we study the temperature dependence of the mutual coherence between different WPs. Since our system is far from equilibrium it does not have a well-defined temperature; yet we can have some insight on the thermal robustness of the polariton condensate coherence by studying the evolution of the interference fringes' visibility with the lattice temperature. We will focus our

attention on three time delays of particular interest. In momentum-space, we evaluate the interference obtained at two different time intervals; at t_1 , from 13 ps to 39 ps, when the four WPs acquire a constant maximum momentum, and at the interval t_3 , from 42 ps to 57 ps, where R_1 and L_2 have decreased their speed and reduced their momentum down to $k \sim 0$. We also investigate the interference pattern in real-space, resulting from the meeting of the WPs R_1 and L_2 around $x \sim 0$ at the interval t_2 , from 22 ps to 37 ps.

To analyze the data and obtain the period and amplitude of the interference fringes, we perform a detailed Fourier analysis of these patterns, to which a baseline is subtracted in order to obtain a cleaner interferogram. As an example, Fig. 2(a) depicts the profile of the emission, integrated in the time interval t_1 , in the full range of momenta, at $T = 10$ K, revealing clear oscillations related to the interference fringes. Fig. 2(b) displays the same profile after the baseline subtraction. Its Fourier analysis, depicted in Fig. 2(c), obtains the amplitudes of the different periods present in the interference pattern, $\kappa \equiv \Delta k$, and reveals a peak corresponding to the predominant period in momentum-space, κ_0 . This period is related to

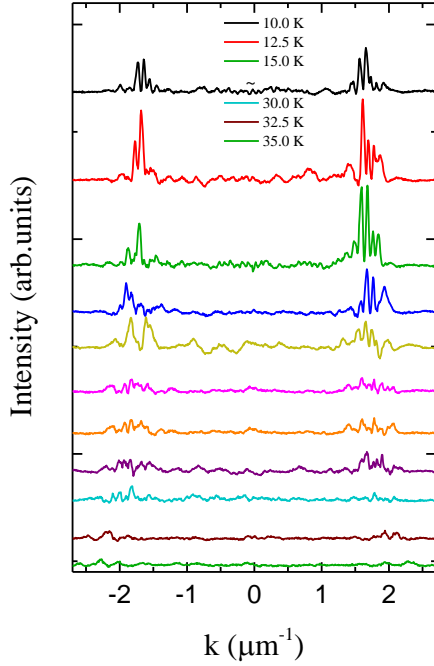


Figure 3. Profile of the emission spectra for t_1 in momentum-space varying the temperature from 10 K (top) to 35 K (bottom) in steps of 2.5 K (only the first and last three temperatures are labelled).

the distance (d) between both excitation spots, S_1 and S_2 , by $\kappa_0 = 2\pi/d$ [27]. The visibility of the fringes shown in Fig. 2(b), is also computed as

$$v = \frac{\sum_{i=1}^n \left(\frac{I_{max} - I_{min}}{I_{max} + I_{min}} \right)_i}{n},$$
 where $I_{max}(I_{min})$ is the maximum (minimum) intensity of the interference oscillation $\#i$ of the n oscillations observed in the interferogram. This value is used to scale the amplitude given by the Fourier analysis for each time interval, as depicted in Fig. 2(c).

We perform a similar analysis of the interferograms obtained for different temperatures. The profiles of the baseline-subtracted emission intensity versus k for t_1 , measured at different temperatures, in steps of 2.5 K, are compiled in Fig. 3. The interference fringes are directly observed in the range of maximum momentum of the PL emission. Above ~ 32.5 K, the lifetime of the polaritons is drastically reduced, hindering their propagation, as demonstrated by the strong reduction of the PL at large $|k|$ values. This also results in the

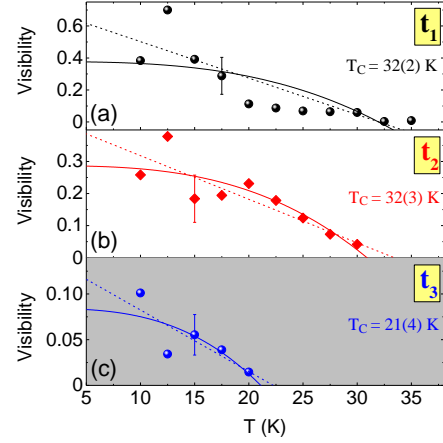


Figure 4. Temperature dependence of the visibility of the interference fringes: in momentum-space for the interval t_1 (black), in the vicinity of $k = 0$ at t_3 (blue) and in real-space at the first crossing of the wavepackets, R_1 and L_2 , t_2 (red). The lines represent fits of the data with $v(T) = v_0 [1 - (T/T_c)^\beta]$, for $\beta=1$ (dotted line) and $\beta=3$ (solid line).

disappearance of the interference fringes. The analysis yields a temperature-independent period of the interferences $\kappa_0 = 0.089(6) \mu\text{m}^{-1}$, indicating a distance in real-space between the moving condensates of $71(5) \mu\text{m}$. The T -independence of κ_0 is expected from the experimental fact that the separation between the two excitation laser-beams is kept constant at $d = 70(1) \mu\text{m}$ for all temperatures. Figure 4 displays the visibility of the fringes (v) versus T : v decays indicating a loss of coherence with increasing temperature. We interpret this reduction of the visibility as a signature of a BEC-like transition and obtain the characteristic critical temperature, $T_c^{t_1} = 32(2) \text{ K}$, from its value when v vanishes [see Fig. 4(a)].

We find a similar visibility reduction when we turn our attention to the interference pattern obtained at t_3 , when R_1 and L_2 meet in momentum-space at $k \sim 0$, resulting in a second set of fringes. In this case, the Fourier analysis gives a period of $\kappa_0 = 0.106(2) \mu\text{m}^{-1}$ corresponding to a distance of $59(1) \mu\text{m}$. This can be directly checked looking at the real-space measurements that reveal a distance between WPs R_1 and L_2 of $d_2 = 60(1) \mu\text{m}$ (Fig. 1(a)). For

this time interval, the signal to noise ratio limits the temperature range in which a reliable Fourier analysis can be performed, so only temperatures below 20 K have been considered. The temperature dependence of the visibility, reveals a similar decay to that obtained for t_1 . However, the visibility decay with temperature is much faster than for t_1 , obtaining a critical temperature of $T_C^{t_3} = 21(4)$ K [see Fig. 4(c)]. Furthermore, for a given temperature, the value of the visibility at t_3 is significantly smaller than that obtained at t_1 , revealing that the coherence gradually decreases with time as the polaritons travel along the sample. The robustness of coherence with temperature is reduced for this time interval since the WPs are in close proximity to the excitonic reservoirs, which contribute to a faster decoherence through exciton-polariton scattering [39-41].

For the sake of completeness, we have also analyzed the interference patterns observed in real-space at t_2 , when R_1 and L_2 meet at $x \sim 0$ [see Fig. 1(a)]. Now, the period of the interference fringes, ξ , is related to the distance in k between WPs R_1 and L_2 , given by $\xi = 2\pi/|\vec{k}_{R_1} - \vec{k}_{L_2}|$ [27]. From our Fourier analysis, we obtain $\xi = 1.8(1) \mu\text{m}$; i.e. $|\vec{k}_{R_1} - \vec{k}_{L_2}| = 3.4(2) \mu\text{m}^{-1}$; and taking into account that $|\vec{k}_{R_1}| = |\vec{k}_{L_2}|$ for $t < 42$ ps, this yields $|\vec{k}_{R_1}| = |\vec{k}_{L_2}| = 1.7(1) \mu\text{m}^{-1}$. This value is in very good agreement with the maximum k value $|\vec{k}_{R_1}| = |\vec{k}_{L_2}| = 1.70(2) \mu\text{m}^{-1}$ directly measured (see Fig 1(b)). In this case, the analysis can be performed just up to 30 K due to lifetime constraints. Red points in Fig. 4(b) compile the temperature dependence of the visibility in real-space: the general behavior of the coherence with increasing temperature is similar to that observed in momentum-space, as expected from the connection between real- and k -space. From the fits of these data, obtained at t_2 , we found $T_C^{t_2} = 32(3)$ K.

Very few studies of the temperature dependence of condensate's coherence can be found in the literature. Two situations have been theoretically considered, to the best of our knowledge, for atomic condensates: i) a refined

description of a 3D cold atom gas confined in a cigar-like trap [42] and ii) a mean field approach for a purely 2D atom gas [43]. In both cases, the temperature dependence of the fraction of condensed atoms takes the general form:

$$n_c(T) = n_0 \left[1 - \left(\frac{T}{T_C} \right)^\beta \right]$$

where T_C is a transition temperature for condensation. In the former approach β is close to 3 while in the latter $\beta \sim 1$. Lacking a detailed theory for non-equilibrium polariton condensates, we test the validity of both atomic theories comparing the behavior of the temperature dependence of the condensed fraction for both models with our results for the visibility of the non-equilibrium polariton condensates. As shown in Fig. 4 both models fit reasonably well our experimental results. Therefore, it is difficult to discriminate among these two approaches and to conclude which model describes more appropriately the temperature dependence of the coherence. It should be also mentioned that in the theoretical models the condensate fraction (and therefore the visibility) is 1 at zero temperature, while our experiments obtain a low-temperature value of the visibility well below 1. This originates from the omnipresence of thermal, non-condensed polaritons [44] and from the non-equilibrium nature of the polariton condensates, implying that, even at extremely low temperature, there are significant effects arising from out-of-equilibrium noise. In any case, independently of the model used to account for the temperature dependence of the coherence, the experimental data yield directly T_C , with an accuracy of ± 1.5 K, from the temperature at which the visibility dies out.

III. CONCLUSIONS

In conclusion, we have investigated the temperature dependence of the mutual coherence of polaritons condensates created separately in real-space in semiconductor microcavity-ridges. At low temperature, a conspicuous phase correlation is observed during the full propagation of the WPs, revealed by the presence of interference fringes in the whole range of the momentum emission. The temperature

dependence of the coherence has been evaluated, through the visibility of the interference patterns, at three different time-delays after the condensate formation. A similar decrease of the coherence with increasing temperature has been found, both in real- and momentum-space that is correlated with the BEC-like transition. A comparison with two theoretical models developed for atomic condensates does not provide a clear conclusion about which model is more appropriate. Moreover, significant differences can be expected when comparing theories developed for equilibrium condensates with polariton condensates, what demands for a more adequate model that take into account the non-equilibrium nature of the polariton condensates.

ACKNOWLEDGMENTS

E.R. acknowledge financial support from a Spanish FPI scholarship BES-2015-074708. This work was partially supported by the Spanish MINECO MAT2014-53119-C2-1-R and P.G.S. acknowledges Funding from the POLAFLOW ERC Starting Grant.

References

- [1] S.I. Pekar, J. Phys. Chem. Solids **5**, 11–22 (1958).
- [2] C. Weisbuch *et al.*, Phys. Rev. Lett. **69**, 3314–3317 (1992).
- [3] A. Bramati *et al.*, Springer Science & Business Media **177**, (2013).
- [4] J. Kasprzak *et al.*, Nature **443**, 409–414 (2006).
- [5] R. Balili *et al.*, Science **316**, 1007–1010 (2007).
- [6] I.L. Aleiner *et al.*, Phys. Rev. B **85**, 121301 (2012).
- [7] T. Byrnes *et al.*, Nat. Phys. **10**, 803–813 (2014).
- [8] D. Caputo *et al.*, arXiv preprint arXiv:1610.05737, (2016).
- [9] I. Carusotto *et al.*, Phys. Rev. B **72**, 125335 (2005).
- [10] G. Christmann *et al.*, New J. Phys. **16**, 103039 (2014).
- [11] K. S. Daskalakis *et al.*, Phys. Rev. Lett. **115**, 035301 (2015).
- [12] A.A. Demenev *et al.*, Phys. Rev. B **94**, 195302 (2016).
- [13] H. Deng *et al.*, Phys. Rev. Lett. **99**, 126403 (2007).
- [14] A. Hayat *et al.*, Opt. Express **22**, 30559–30570 (2014).
- [15] R. Houdré *et al.*, Phys. Rev. B **61**, R13333 (2000).
- [16] K. Ji *et al.*, Phys. Rev. B **91**, 045301 (2015).
- [17] S. Kim *et al.*, Phys. Rev. X **6**, 011026 (2016).
- [18] K.G. Lagoudakis *et al.*, Phys. Rev. Lett. **105**, 120403 (2010).
- [19] F.P. Laussy *et al.*, J. Phys.: Cond. Matter **16**, S3665 (2004).
- [20] M. Richard *et al.*, Phys. Rev. Lett. **94**, 187401 (2005).
- [21] D. Snoke *et al.*, Science **298**, 1368–1372 (2002).
- [22] R. Spano *et al.*, New J. Phys. **14**, 075018 (2012).
- [23] D.M. Whittaker *et al.*, Europhys. Lett. **87**, 27002 (2009).
- [24] J. Fischer *et al.*, Phys. Rev. Lett. **113**, 203902 (2014).
- [25] A. A. High *et al.*, Nature **483**, 584–588 (2012).
- [26] M. R. Andrews, Science **275**, 637–641 (1997).
- [27] C. Antón *et al.*, Phys. Rev. B **90**, 155311 (2014).
- [28] I. Bloch *et al.*, Nature **403**, 166–170 (2000).
- [29] R. Gati *et al.*, New J. Phys. **8**, 189 (2006).
- [30] R. Gati *et al.*, Phys. Rev. Lett. **96**, 130404 (2006).
- [31] J. Mayers, J. Phys. A: Math. Theor. **47**, 395302 (2014).
- [32] M. E. Lebedev, Sci. Rep. **7**, 9515 (2017).
- [33] C. Ouellet-Plamondon *et al.*, Phys. Rev. B **95**, 085302 (2017).
- [34] G. Tosi *et al.*, Nat. Phys. **8**, 190–194 (2012).
- [35] P. Tsotsis *et al.*, New J. Phys. **14**, 023060 (2012).
- [36] C. Antón *et al.*, Phys. Rev. B **91**, 075305 (2015).
- [37] E. Wertz *et al.*, Phys. Rev. Lett. **109**, 216404 (2012).
- [38] E. Wertz *et al.*, Nature Phys. **6**, 860 (2010).
- [39] P.G. Savvidis *et al.*, Phys. Rev. B **64**, 075311 (2001).
- [40] D. Porras *et al.*, Phys. Rev. B **66**, 085304 (2002).
- [41] G. Dasbach *et al.*, Phys. Rev. B **62**, 13076 (2000).
- [42] S. Giorgini *et al.*, Phys. Rev. A **54**, R4633 (1996).
- [43] N. Prokof'ev and B. Svistunov, Phys. Rev. A **66**, 043608 (2002).
- [44] E. del Valle *et al.*, Phys. Rev. Lett. **103**, 096404 (2009).